Adsorption (2008) 14: 475–484
DOI 10.1007/s10450-008-9132-y

Co-diffusion with a slow species in zeolites: cyclic experimentation and advanced modeling

K. Lettat · E. Jolimaitre · M. Tayakout · A. Methivier · D. Tondeur

Received: 2 May 2007 / Revised: 26 October 2007 / Accepted: 18 April 2008 / Published online: 22 May 2008

Abstract In this study, a new experimental method based on cyclic breakthrough curves is presented, in order to estimate the co-diffusion coefficients for mixtures at high adsorption loadings. For this purpose, cyclic liquid phase breakthrough curves of mixtures of 2-methylpentane 3-methylpentane (fast-diffusing species) and 2,2-dimethylbutane (slow-diffusing species) have been measured experimentally for different feed compositions at 185°C.

Estimation of Langmuir coefficients and self-diffusivities was attempted from simple binary breakthrough curves with the above components using a modified Maxwell-Stefan-type model. However, for the slow-diffusing species, the parameters cannot be estimated accurately from such experiments, because the quantity of 22DMB entering the zeolite network in the experiment duration is not sufficient.

On the other hand, a clear influence of the slow diffusing species (22DMB) on the fast diffusing species (3MP) breakthrough curves during cycles has been demonstrated. This phenomenon confirms that 22DMB slowly accumulates in the adsorbent during the cycles, and that is becomes therefore possible to estimate the 22DMB parameters from the cyclic data.

Keywords Liquid-phase diffusion · Experimental study · Dusty gas model · Maxwell-Stefan equations · Silicalite · Paraffins

K. Lettat · E. Jolimaitre (✉) · M. Tayakout · A. Methivier
Division Catalyse et Séparation, IFP Lyon, Vernaison 69390, France
e-mail: elsa.jolimaitre@ifp.fr

K. Lettat · D. Tondeur
Laboratoire des Sciences du Génie Chimique-CNRS, Nancy-Université, Nancy, France

1 Introduction

Separation of doubled-branched paraffins from mono-branched and normal paraffins is of great industrial interest, because of its potential applications in the octane number enhancement of fuel products. A potential separation technique would be an adsorption process based on the difference in the kinetics of diffusion between mono and di-branched molecules. This is possible only if the pores of the adsorbent have a diameter close to the diameter of the molecules to be separated. Therefore, this kinetic-based separation has been investigated using silicalite adsorbent.

To correctly scale-up this adsorption separation process and to predict its performance, it is necessary that the investigation take place under industrial conditions, i.e. at high adsorption loading. However, most of the articles in the literature present only experimental results in the gas phase at low loading (Barcia et al. 2006; Calvacante and Ruthven 1995; Jolimaitre 1999; Millot 1998; Schuring et al. 2001).

Despite its great industrial interest, only few articles have been published regarding liquid phase adsorption (Boulicaut et al. 1998; Choudhary et al. 1989; Uguina et al. 2006; Yu et al. 2005). This is due to the fact that the classical techniques are not well adapted to the measurement of slow diffusing species, such as di-branched paraffins in silicalite, leading to important experimental incertitude. The difficulties are even more important for the simultaneous measurement of very different diffusion coefficients. Indeed, the optimal experimental conditions for fast species are quite different from that for slow-diffusing species. Also, when separation is operated in the liquid phase, the adsorbent microporosity is fully occupied. Volume constraints in the zeolite micropores, which can be neglected at low loadings, have then to be taken into account in the modeling and analysis.

The aim of this work is to develop a new experimental method to characterize the co-diffusion of slow and fast-diffusing species at saturation of the adsorbent. The chosen experimental method is based on the measurement of the output of an adsorbent column subjected to cyclic injections of the mixture to be studied and of a desorbent molecule. Firstly, a set of binary and ternary breakthrough experiments is carried out, allowing a rough estimation of equilibrium parameters and diffusion coefficients. Secondly, it is shown that cyclic experiments enhance the long term effects of the slow-diffusing species, and allow to improve the parameter estimation procedure. The analysis of the experimental results is carried out using a detailed mathematical model of the micropore diffusion process, including Maxwell-Stefan coupling of single file diffusion with volume constraints and Langmuir isotherms.

2 Model

The model used for this work has been thoroughly described in a separate paper (Tayakout et al. 2007). Consequently, only the main assumptions and equations will be presented here.

2.1 Model assumptions

In order to minimize the pressure drop, the adsorption column is packed with bi-disperse pellets composed of zeolite crystals held together by a binder. The pellets and the microporous crystals are supposed to be spherical. We define three levels of porosity in the column: the bulk fluid (extra-granular fluid phase), the fluid-filled macroporosity of the pellets, and the crystals containing the microporosity where adsorption occurs (Ruthven 1984).

The liquid mixture is ideal, the molar volumes of the different molecules are assumed to be identical, and all species have the same heat of adsorption, which implies that the bed is isothermal. All these assumptions are realistic only because the studied species are isomers having very close physical properties.

The axial dispersion in the extragranular liquid phase is considered to be small. The flow in the packed bed can therefore be represented by a cascade of CSTR in series (40 CSTR). Mass transfer resistances at the pellet surface and in the macropores are lumped into a single external film mass-transfer coefficient k^m. A stagnant film around the zeolite crystals is also introduced, with a corresponding mass-transfer coefficient k^c. The number of CSTR and the two film mass transfer coefficients have been estimated in a previous study (Tayakout et al. 2007), using experiments with a non-adsorbable species (1,3,5-triisopropylbenzene, TiPB) and considering that the dispersion of the TiPB breakthrough curve was only due to axial dispersion in the extra-granular fluid phase.

All the molecules in the micropores are in the adsorbed phase and diffusion occurs in that state (no fluid-phase in the crystals). This is justified by the diameter of the micropores which is very close to the molecular kinetic diameters. The molar volumes in the liquid and in the adsorbed phase are assumed to be the same. The adsorbed phase is always saturated; this implies that one molecule can be adsorbed only if another molecule is desorbed at the same time. Therefore, it is assumed that there is no variation of the fluid phase velocity along the column.

The adsorption equilibrium is represented by the generalized Langmuir model, with the same adsorption capacities for all adsorbates. The intra-crystalline transport model described later in this paper is based on the Maxwell-Stefan equation for diffusion in a porous solid (Dusty Gas Model), as published by Krishna (1990), but adapted to our operating conditions (saturation of adsorbent implying a constraint on the total adsorbed volume, single file diffusion…).

2.2 Equations

The model equations are derived from mass balances for the three levels of porosity of the bed, subject to the above assumptions. The equations are written in volume fractions ϕ, with subscripts corresponding to the species, the first superscript to the phase, $f$luid, $m$acropore or $c$rystal, and the second superscript to the index of the CSTR; Nc designates the number of components. ϕ^f is expressed as a volume fraction of the extra-granular fluid, ϕ^m as a volume fraction of the macropores and ϕ^c as a volume fraction of the crystals.

2.2.1 *Fluid phase*

$$\begin{bmatrix} \frac{L}{u^f}\frac{\partial \phi_1^{f,i}}{\partial t} \\ \vdots \\ \frac{L}{u^f}\frac{\partial \phi_{Nc-1}^{f,i}}{\partial t} \end{bmatrix} = \begin{bmatrix} (\phi_1^{f,i-1} - \phi_1^{f,i}) + \frac{L}{u^f}\frac{3(1-\varepsilon_i)\varepsilon_p}{\varepsilon_i R_p} k_1^m (\phi_1^{m,i} - \phi_1^{f,i}) \\ \vdots \\ (\phi_{Nc-1}^{f,i-1} - \phi_{Nc-1}^{f,i}) + \frac{L}{u^f}\frac{3(1-\varepsilon_i)\varepsilon_p}{\varepsilon_i R_P} k_{Nc-1}^m (\phi_{Nc-1}^{m,i} - \phi_{Nc-1}^{f,i}) \end{bmatrix} \tag{1}$$

with $\sum_{j=1}^{Nc} \phi_j^{f,i} = 1, i = 1, \ldots, N_{CSTR}$.

2.2.2 Macropore mass balance

$$\begin{bmatrix} \frac{\partial \phi_1^{m,i}}{\partial t} \\ \vdots \\ \frac{\partial \phi_{Nc-1}^{m,i}}{\partial t} \end{bmatrix} = \begin{bmatrix} -\frac{3}{R_p} k_1^m (\phi_1^{m,i} - \phi_1^{f,i}) - \frac{3(1-\varepsilon_p)}{\varepsilon_p R_c} k_1^c (\phi_1^{m,i} - \phi_1^{*,i}) \\ \vdots \\ -\frac{3}{R_p} k_1^m (\phi_{Nc-1}^{m,i} - \phi_{Nc-1}^{f,i}) - \frac{3(1-\varepsilon_p)}{\varepsilon_p R_c} k_{Nc-1}^c (\phi_{Nc-1}^{m,i} - \phi_{Nc-1}^{*,i}) \end{bmatrix} \tag{2}$$

with $\sum_{j=1}^{Nc} \phi_j^{m,i} = 1, i = 1, \ldots, N_{CSTR}$.

2.2.3 Crystal mass balance

$$\frac{\partial \phi_j^{c,i}}{v \cdot \partial t} = -\frac{1}{r^2} \frac{\partial (r^2 N_j^{c,i})}{\partial r} \quad j = 1, \ldots, Nc+1 \tag{3}$$

with $\sum_{j=1}^{Nc+1} \phi_j^{c,i} = 1$, $i = 1, \ldots, N_{CSTR}$, and $\sum_{j=1}^{Nc+1} N_j^{c,i} = 0, i = 1, \ldots, N_{CSTR}$.

2.2.4 Thermodynamic equilibrium conditions

The state variable chosen to describe equilibrium in the present model is the fictitious fluid phase variable ϕ^* in equilibrium with the adsorbed phase ϕ^c.

$$\phi_j^{c,i} = \frac{q_{sat} b_j \phi_j^{*,i}}{1 + \sum_{k=1}^{Nc} \frac{b_k \phi_k^{*,i}}{v}} \quad j = 1, \ldots, Nc+1 \text{ and } i = 1, \ldots, N_{CSTR} \tag{4}$$

2.2.5 Expression of the diffusion in the micropores

To complete this model, an expression for the diffusion fluxes in the micropores N^c has to be established. Our model is based on the Maxwell-Stefan equation (Krishna 1990) coupled with the Gibbs-Duhem relation, the equilibrium law and the material balance in the crystals. The size of the diffusing molecules being very close to the pore radius, it is assumed that there is no possibility of counter-exchange between two adsorbed species i and j inside a given pore. Therefore, the binary diffusion coefficients are not taken into account ($D_{ij} = 0$) and it is assumed that only single file diffusion occur in the crystal lattice. To preserve the independence of self-diffusion coefficients for each species, the flux of the solid N_{Nc+1}^c is taken into account in this model.

Adding the saturation constraint in the adsorbed phase, the Maxwell-Stefan equation gives:

$$\begin{aligned} &\frac{\phi_j^{c,i}}{RT} \nabla_{T,P} \mu_j^{c,i} \\ &\quad = -\frac{1}{q_{sat}} \frac{1}{D_{j,Nc+1}} (\phi_{Nc+1}^{c,i} \cdot N_j^{c,i} - \phi_j^{c,i} \cdot N_{Nc+1}^{c,i}) \\ &\qquad j = 1, \ldots, Nc+1; \; i = 1, \ldots, N_{CSTR} \\ &\sum_{j=1}^{Nc+1} \phi_j^c = 1 \\ &\quad \text{(volume constraint } s \text{ in the micropores)} \\ &\sum_{j=1}^{Nc+1} N_j^c = 0 \\ &\quad \text{(diffusion fluxes constraint } s \text{ in the micropores)} \\ &\sum_{j=1}^{Nc+1} q_j \nabla \mu_j = 0 \\ &\quad \text{(Gibbs-Duhem relation applied to the adsorbed phase)} \end{aligned} \tag{5}$$

The constraints of (5) and the equilibrium law (4) are substituted into the Maxwell-Stefan equation to yield the following system of equations, relating the gradients of the fictitious fluid phase concentrations to the fluxes via a coupling matrix of dimension $Nc \times Nc$:

$$\begin{bmatrix} q_{sat} b_1 \frac{\partial \phi_1^{*,i}}{\partial r} \\ \vdots \\ q_{sat} b_{Nc} \frac{\partial \phi_{Nc}^{*,i}}{\partial r} \end{bmatrix} = - \begin{bmatrix} \frac{1}{D_{1,Nc+1}} \left(\frac{1 + \sum_{k=1}^{Nc} b_k \frac{\phi_k^{*,i}}{v}}{q_{sat}} - \sum_{l=2}^{Nc} b_l \phi_l^{*,i} \right) & \cdots & \left(\frac{b_1 \phi_1^{*,i}}{D_{1,Nc+1}} \right) \\ \vdots & \ddots & \vdots \\ \left(\frac{b_{Nc} \phi_{Nc}^{*,i}}{D_{Nc,Nc+1}} \right) & \cdots & \frac{1}{D_{Nc,Nc+1}} \left(\frac{1 + \sum_{k=1}^{Nc} b_k \frac{\phi_k^{*,i}}{v}}{q_{sat}} - \sum_{l=1}^{Nc-1} b_l \phi_l^{*,i} \right) \end{bmatrix} \times \begin{bmatrix} N_1^{c,i} \\ \vdots \\ N_{Nc}^{c,i} \end{bmatrix} \tag{6}$$

We observe that, although there are only *Nc* individual (single-file) diffusion coefficients, the system is fully coupled through the equilibrium.

2.3 Numerical method of resolution

The set of partial differential equations is first reduced to a set of ordinary differential equations by applying an orthogonal collocation technique to the spatial coordinate corresponding to the crystal radius, using subroutines JCOBI and DFOPR developed by Villadsen and Michelsen (1978). The resulting ordinary differential-algebraic system of equations is solved using the DDASPG integration subroutine (IMSL library), based on the Petzold-Gear BDF method. The matrix (6) is inverted by the DLINRG inversion subroutine (IMSL library).

3 Experimental

3.1 Adsorbent characterization

The silicalite crystals used in this study were supplied by Zeolyst International. The Si/Al ratio, measured by X-ray fluorescence, is $500 \pm 50\%$. The few H^+ cations were replaced by Na^+ cations using the conventional ion exchange technique and subsequent washing. Scanning electron microscopy showed that they consisted of spherical crystals with mean crystal radius of $R_c = 0{,}75 \cdot 10^{-6}$ m.

This zeolite was pelletized with a silica binder in the Institut Français du Pétrole, then cut and sieved. Extrudates are small cylinders with a diameter of 0,85 mm and a mean length of 0,8 mm. For model simplification, particles were supposed to be spherical with a mean radius of $R_P = 4{,}1 \cdot 10^{-4}$ m. The binder ratio, determined from n-hexane adsorption gravimetric uptake experiments performed with both crystals and particles, is 20%.

Prior to experiments, the sample was activated in a nitrogen stream for 3 h at 300°C.

3.2 Adsorbates

2-methylpentane (2MP) and 3-methylpentane (3MP) were purchased from Fluka Chemika. 2,3-dimethylbutane (23DMB) and 2,2-dimethylbutane (22DMB) were purchased from SAFC. The specified purities are over 99%.

3.3 Experimental setup

A stainless steel column ($L_{bed} = 1$ m and $d_{col} = 1{,}04 \cdot 10^{-2}$ m) is filled with a known mass of particles and placed into an oven. First the column is filled with the solvent (or desorbent) which is also an adsorbable species until it is fully degassed. Then the feed is pumped into the column with a GILSON pump (0–25 mL/min) until complete breakthrough (outlet concentration = inlet concentration). The liquid flow rate is measured with a Bronkhorst mass flow meter at the outlet of the column. During the experiment the whole column is maintained at 35 bar and 185°C. Liquid fractions of the effluent are collected and analyzed by a gas chromatograph with FID detector and PONA analytical column. The concentrations at the outlet of the column are plotted as fractional volumes as a function of time; they are called "breakthrough curves". A reverse breakthrough experiment consists in injecting the solvent into a column filled with the feed. This set-up is used in cyclic mode by injecting alternatively the feed and the solvent into the adsorbent column (Fig. 1).

In this study, we focused on the breakthrough of binary 3MP/22DMB mixtures of different compositions, exchanging with 2MP, the desorbent. First, we studied only pure 3MP and 22DMB breakthrough curves (respectively run 1 and 2). Run 3 and 4 were then performed with respectively a 50/50 and a 30/70 molar % 3MP/22DMB mixture. Experimental conditions common to all the breakthrough experiments are given in Table 1.

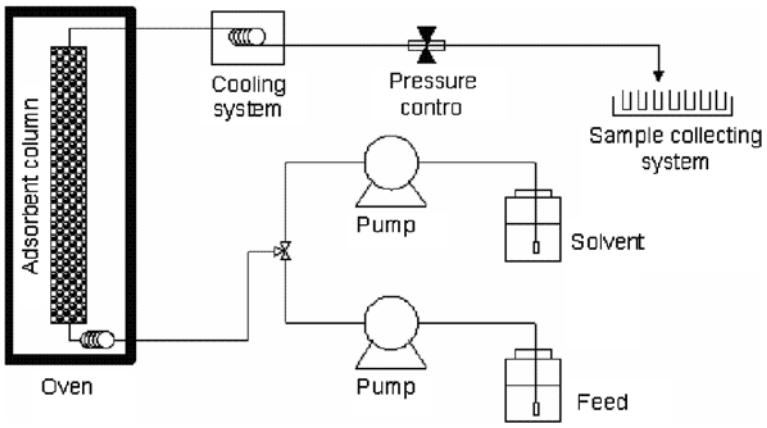

Fig. 1 Experimental set-up

4 Results and discussion

For each experimental condition, the simulated results (solid lines) will be presented along with the experimental points.

Table 1 Experimental conditions

Feed (molar %)	3MP/22DMB
Run 1	100/0
Run 2	0/100
Run 3	50/50
Run 4	30/70
Desorbent	2MP
Flow (mL/min)	10
Duration (min/breakthrough)	15
T column (°C)	185
Pressure (bar)	35
Mass of solid (g)	74,6
Column volume (mL)	84,8
Dead volume (mL)	12,0

Table 2 Input parameters of the model

Parameters	Values
u^f (m/s)	$6{,}75 \cdot 10^{-3}$
ε_i (extra-granular porosity, referred to the bed volume)	0,29
ε_p (intra-particle porosity, referred to the pellet volume)	0,40
v (m^3/mol)	$1{,}9 \cdot 10^{-4}$
R_c (m)	$0{,}75 \cdot 10^{-6}$
R_p (m)	$0{,}41 \cdot 10^{-3}$
q_{sat} (mol/m^3)	1250
k^m (m/s)	$8 \cdot 10^{-4}$
k^c (m/s)	$9 \cdot 10^{-3}$

The input parameters, common to all the simulations, are summarized in Table 2. As mentioned before, the particles and crystals film mass transfer coefficients have been estimated previously using a set of breakthrough curves for a non adsorbable species (1,3,5-triisopropylbenzene) as indicated in Tayakout et al. (2007). Only the Langmuir coefficient, b_j, and the single-file-diffusion coefficient, $D_{j,Nc+1}$ have been estimated from our experimental curves. For the mono-branched isomers, the parameters have been estimated from run 1 and for 22DMB from run 2. The final estimated values used in the simulations are given in Table 3.

4.1 Pure components breakthrough curves

4.1.1 Mono-branched paraffins (3MP vs 2MP)

Figure 2 shows a complete breakthrough curve (adsorption + desorption) of 3MP in 2MP. The left-hand side of the figure represents the breakthrough of 3MP (reverse breakthrough of 2MP), and the right-hand side of the figure the reverse breakthrough of 3MP (breakthrough of 2MP). It can be seen on Fig. 2 (and it is verified quantitatively) that the breakthrough and reverse breakthrough curves are perfectly symmetrical for the two components, meaning that the two mono-branched components have similar behaviors and can be represented by the same set of b_j and $D_{j,Nc+1}$ values. The best simulation fit (the solid line), was obtained for a Langmuir coefficient b of 1,0 m^3/mol, and an internal single-file-diffusion coefficient of $1 \cdot 10^{-14}$ m^2/s for both components.

Table 3 Estimated Langmuir parameter and diffusion coefficients

	b_j (m^3/mol)	$D_{j,Nc+1}$ (m^2/s)
3MP	1,0	$1 \cdot 10^{-14}$
22DMB	0,4	$1 \cdot 10^{-16}$
2MP	1,0	$1 \cdot 10^{-14}$

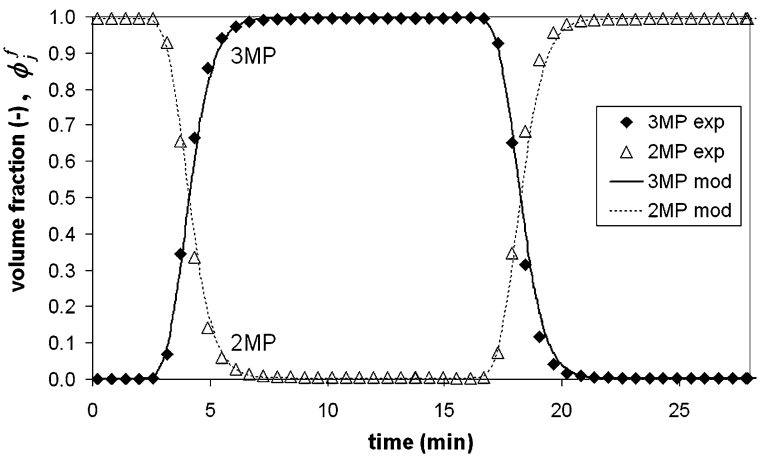

Fig. 2 Experimental and simulated breakthrough curves for run 1 (1 cycle). The experimental conditions and model parameters are specified in Tables 1, 2 and 3. The *lines* represent the model predictions, and the *points* are experimental data

The same experiment was carried-out for several cycles, and one can see on Fig. 3a that no evolution of the breakthrough curves is visible during the cycles. The superimposition of all the curves (Fig. 3b) shows that all the breakthrough curves are perfectly identical. Apart from demonstrating the excellent experimental reproducibility, this result also proves that adsorption equilibrium is attained in the crystal at the end of each breakthrough curve. This is not surprising, since the mono-branched components are fast-diffusing species in silicalite.

4.1.2 Mono and di-branched paraffins (22DMB vs 2MP)

Figures 4a and b show the breakthrough curves and the cycles for pure 22DMB replacing 2MP. First of all, it is interesting to notice that the breakthrough and reverse breakthrough curves are not symmetrical, indicating that the two molecules do not have the same affinity for silicalite. Moreover, the breakthrough curves are much more dispersed than that of 3MP: after 15 minutes, the output composition has not yet reached a stabilized value. This behaviour is characteristic of slow-diffusing species such as di-branched alkanes in silicalite.

The set of parameters used in the simulation are $b_{22DMB} = 0{,}4\ \mathrm{m^3/mol}$ and $D_{22DMB} = 1 \cdot 10^{-16}\ \mathrm{m^2/s}$. These values are coherent with the above remarks: 22DMB is less strongly adsorbed than 2MP and its diffusion coefficient is smaller than that of 2MP by two orders of magnitude. As shown on Fig. 4a, it is difficult to accurately fit the experimental breakthrough curves with only one cycle. In particular, the "tail" of the curve—which contains most of the kinetic information—is not very well-represented by our set of parameters. It is possible that the thermodynamical and kinetic parameters are coupled, making the parameters estimation procedure more complex.

Moreover, as can be seen on Fig. 4b, only a very slight variation of the experimental breakthrough curves is visible during the cycles. It is therefore difficult, to estimate a valuable set of parameters for 22DMB from pure components experiments, even with several cycles. That's why we carried out binary feed breakthrough experiments with mono/di-branched mixtures.

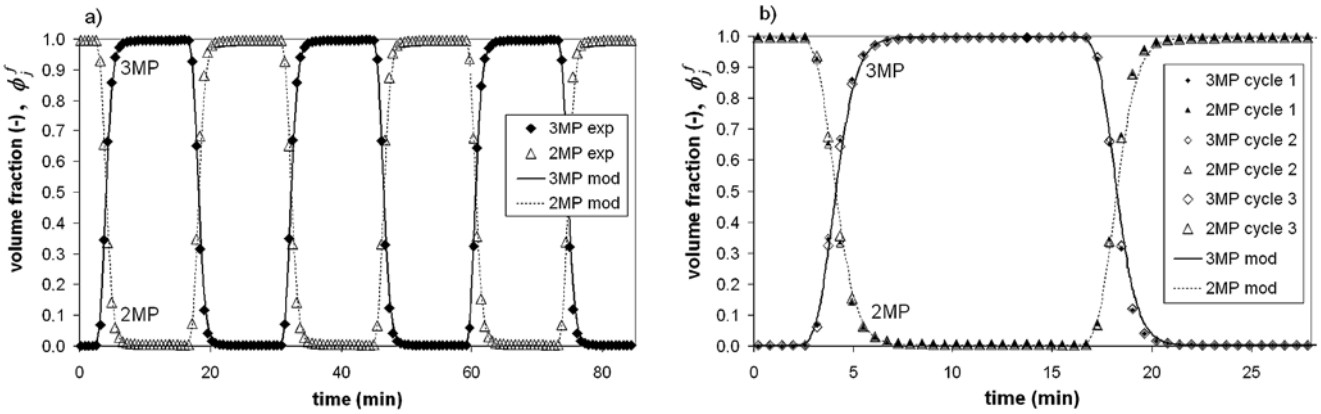

Fig. 3 Experimental and simulated breakthrough curves for run 1 ((**a**): 3 successive cycles; (**b**): 3 superimposed cycles). The experimental conditions and model parameters are specified in Tables 1, 2 and 3. The *lines* represent the model predictions, and the *points* are experimental data

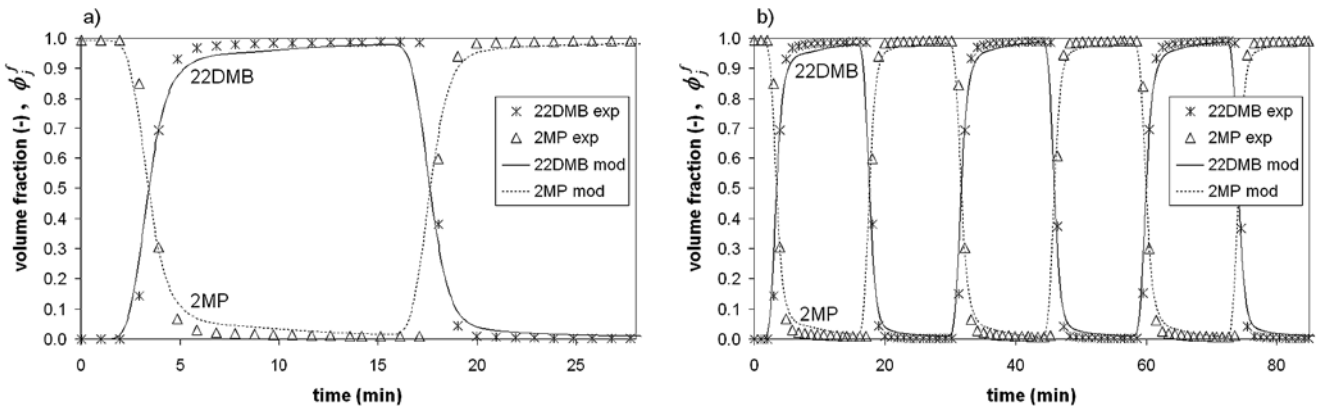

Fig. 4 Experimental and simulated breakthrough curves for run 1 ((**a**): 1 cycle; (**b**): 3 successive cycles). The experimental conditions and model parameters are specified in Tables 1, 2 and 3. The *lines* represent the model predictions, and the *points* are experimental data

4.2 Binary feed breakthrough curves

4.2.1 3MP/22DMB (50/50) and (30/70) vs 2MP

Figures 5a and b show experimental and simulated one cycle breakthrough curves, with the feed consisting respectively of 50/50 and 30/70 mixtures of 3MP and 22DMB. For both mixtures, 22DMB has a smaller breakthrough time than 3MP, meaning that 22DMB is less strongly adsorbed than 3MP. This also entails a roll-up that can be observed on the reverse breakthrough curve of 3MP. This could be predicted from the Langmuir parameters estimated with the pure components curves: the 22DMB Langmuir coefficient is more than 2 times smaller than that of the mono-branched isomers. Indeed, the simulations represent rather well the experimental data (Figs. 5a and b) without further fitting (Table 3).

It may come as a surprise that no visible tailing is observed at the end of the 22DMB breakthrough curve, contrarily to what was observed previously for the single-component breakthrough curves. It is probable that, in presence of 3MP, the amount of 22DMB adsorbed in the crystals is not significant enough to have a visible effect on the curve. This remark is valid for all the 22DMB breakthrough curves, whatever the cycle number (Fig. 6) or the feed composition. The 22DMB shows an apparent behaviour close to that of a non-adsorbable species, and hardly enters the microporosity. As a consequence, it is not possible to estimate the 22DMB diffusion coefficient from these breakthrough curves.

However, there is a visible evolution of the 3MP breakthrough curves as a function of cycles for the feed containing 70% of 22DMB (Figs. 7 and 8). During the cycles, the 3MP roll-up decreases slowly, meaning that the quantity of 3MP desorbed by 2MP (and therefore adsorbed during the adsorption phase) is smaller and smaller. The Fig. 8a shows clearly that this phenomenon is observed during both adsorption and desorption phases, but, due to the presence of the roll-up on the desorption curves, it is more pronounced during the desorption.

This phenomenon is clearly due to the presence of the di-branched molecule, which tends to enter very slowly into the zeolite porosity and to block the entrance of the mono-branched isomers. This is visible only for high 22DMB con-

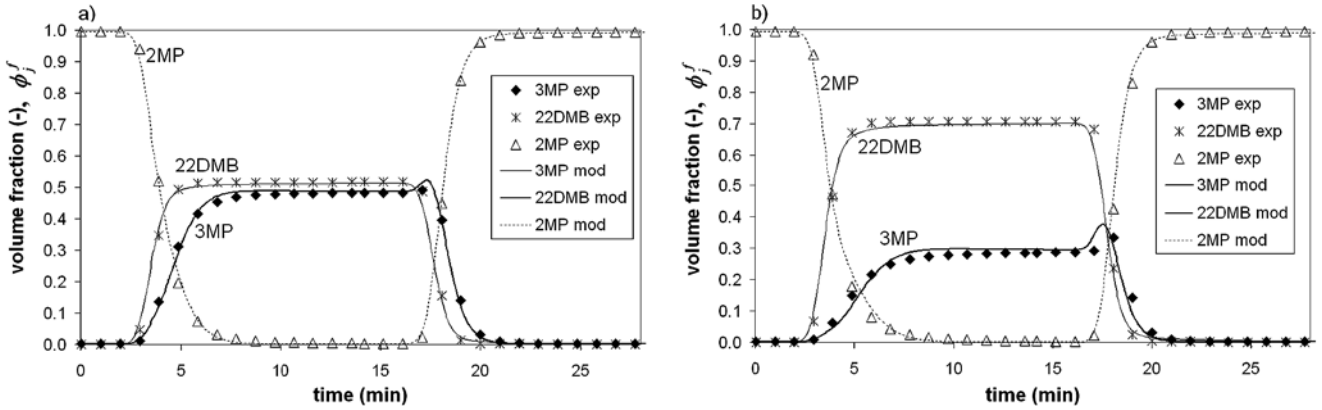

Fig. 5 Experimental and simulated binary breakthrough curves for mixtures 3MP/22DMB at different compositions vs 2MP (1 cycle) ((**a**): run 3; (**b**): run 4). The experimental conditions and model parameters are specified in Tables 1, 2 and 3. The *lines* represent the model predictions, and the *points* are experimental data

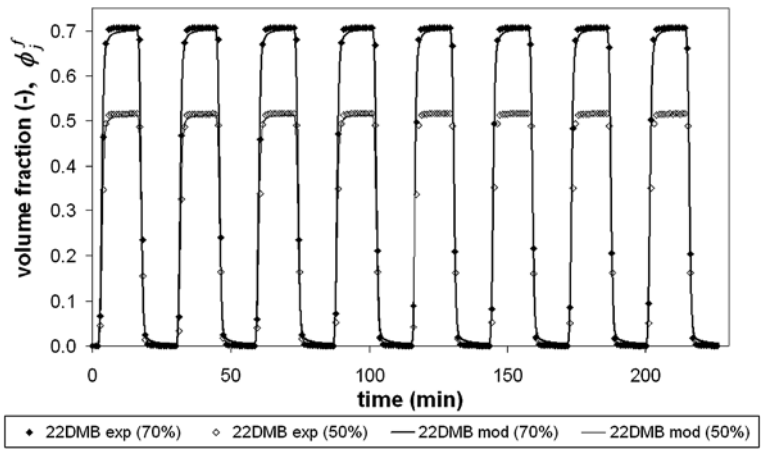

Fig. 6 Experimental and simulated breakthrough curves for 22DMB (50%) and 22DMB (70%) (8 successive cycles). The experimental conditions and model parameters are specified in Tables 1, 2 and 3. The *lines* represent the model predictions, and the *points* are experimental data

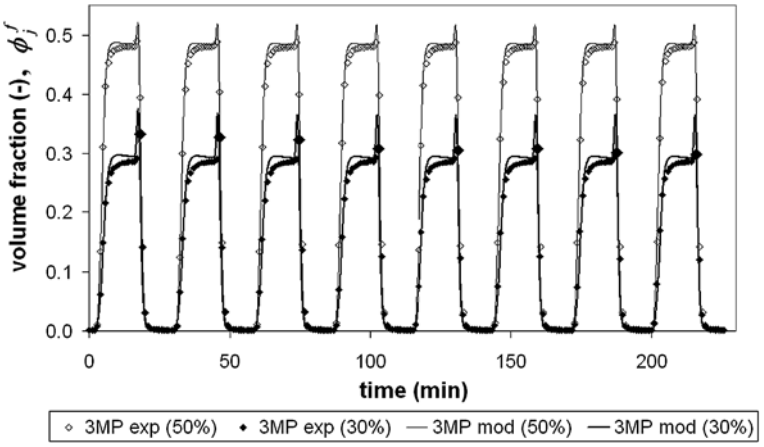

Fig. 7 Experimental and simulated breakthrough curves for 3MP (30%) and 3MP (50%) (8 successive cycles). The experimental conditions and model parameters are specified in Tables 1, 2 and 3. The *lines* represent the model predictions, and the *points* are experimental data

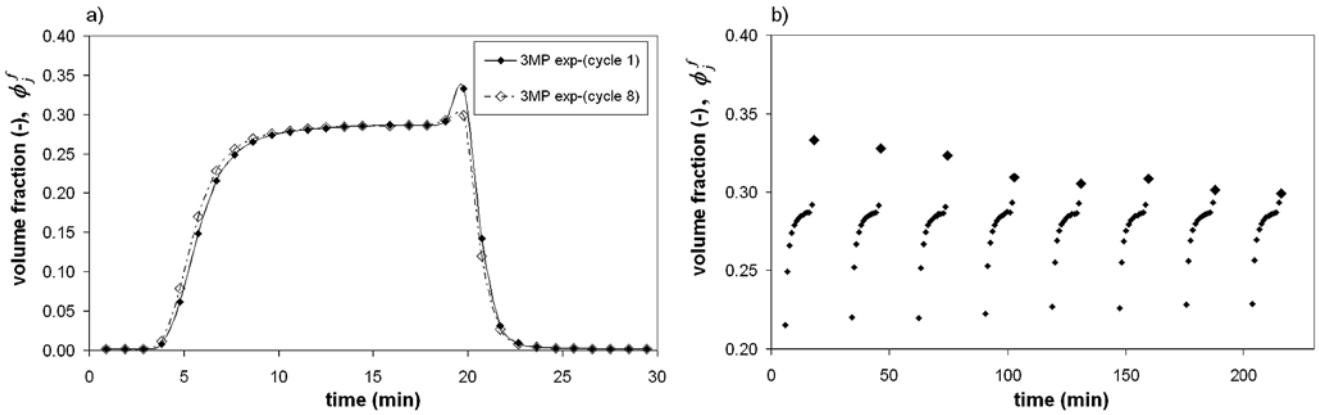

Fig. 8 Experimental breakthrough curves for 3MP 30% (run 4) ((**a**): cycle 1 and cycle 8 superimposed; (**b**): 8 successive cycles). The experimental conditions are specified in Table 1 (run 4)

centration mixtures. Otherwise, the amount of 22DMB adsorbed is so small that the effect of its accumulation in the microporosity is not perceptible.

The cycles were simulated using the previously estimated parameters (see the solid lines on Figs. 6 and 7). Although the model predicts quite well the 22DMB behaviour, the evolution of the 3MP breakthrough curves during the cycles is not well represented. The loss of adsorption capacity for the 3MP (due to the slow accumulation of 22DMB in the zeolite structure) is qualitatively predicted but greatly underestimated by the model. The parameters estimated from the pure-component breakthrough curves cannot represent accurately the cyclic binary behaviour. However, these cyclic results show that the diffusion of 22DMB has a clear and measurable influence on the 3MP breakthrough curve evolution during the cycles, meaning that it is possible to estimate D_{22DMB} from the cycles results. Our next step will therefore consist in estimating the 22DMB parameters from two different experimental results:

1. the single components 22DMB vs 2MP breakthrough curve,
2. the cyclic evolution of the 3MP breakthrough curve in presence of 22DMB.

Using both kinds of experiments will enable a more precise and reliable estimation of the parameters.

This will be possible only if the experimental conditions are fixed such that the variation of the 22DMB adsorbed quantity during the cycles is not negligible. To illustrate this, we have examined the evolution of the solid-phase concentration (expressed here as volume fraction of the crystals), calculated from the simulations and taken at the bed outlet. This quantity is plotted on Fig. 9 as a function of time for the first four cycles, for runs 2, 3 and 4. For the feed containing only 50% of 22DMB (run 3), the 22DMB simulated adsorbed-phase concentration is always smaller than 200 mol/m^3 (indeed, the model predicts that about 15% of the microporosity is filled with 22DMB). Although this quantity is not negligible compared to the saturation concentration in the crystals (1250 mol/m^3), the influence of this accumulation on the mono-branched fluid phase concentration (breakthrough curve) is not clearly visible. However, for the feed containing 70% (run 4), the 22DMB simulated

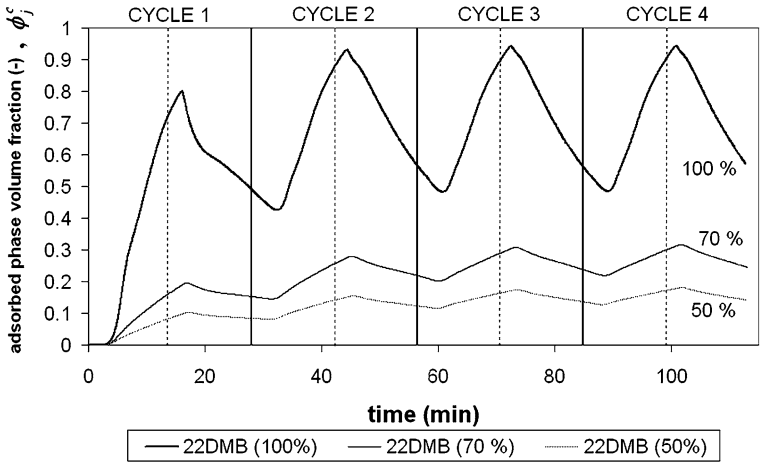

Fig. 9 Simulated adsorbed phase volume fraction curves of 22DMB at the bed outlet for different concentrations (4 successive cycles). The model parameters are specified in Tables 2 and 3

adsorbed-phase volume fraction reaches 30% of the saturation loading (≈400 mol/m^3) and the breakthrough curves vary with the cycles. To fully use the information contained in this transient behavior, it is therefore necessary to choose experimental conditions that will enhance the adsorption of the slow-diffusing species.

5 Conclusion

Cyclic breakthrough curves for the adsorption of mixtures of 2MP, 3MP and 22DMB on silicalite have been measured. Comparison between experiments and simulations has led us to the following conclusions:

1. For pure 22DMB, the 22DMB quantity adsorbed is non negligible (more than 50% of the adsorbent capacity) and the breakthrough curves present a tail, which is characteristic of slow-diffusing species.
2. For binary breakthrough curves, the presence of 22DMB in the feed induces an evolution of the fast-diffusing species (2MP and 3MP) breakthrough curves during the cycles: the quantity of 3MP entering the zeolite decreases as a function of time. This is only true if the quantity of 22DMB in the adsorbed phase is important (more than 70% of 22DMB in the feed).
3. A set of thermodynamic and kinetic parameters for 22DMB was estimated using only the simple binary breakthrough curves. When inserted into the model, this set of parameters predicts qualitatively the decrease of the 3MP roll-up, but does not permit a good quantitative representation of the mono-branched breakthrough curves evolution during the cycles.

Thus, the next step in our study will consist in using all the experimental results, the simple breakthrough curves as well as the cyclic experiments, in order to more precisely estimate the 22DMB parameters. Moreover, the operating conditions (feed composition, flow rate, cycles duration…) will be optimized in order to improve the method sensitivity.

6 Nomenclature

b_i: thermodynamic coefficient of component i (m^3 *of fluid*/mol)
$D_{i,nc+1}$: Maxwell-Stefan diffusion coefficient of component i (m^2/s)
D_{ij}: Maxwell-Stefan binary counter-diffusion coefficient (m^2/s)
d_{col}: Column diameter (m)
k_i^c: mass transfer coefficient of component i corresponding to the crystal (m/s)
k_i^m: mass transfer coefficient of component i corresponding to the macroporosity (m/s)
L: equivalent packed column length for a CSTR ($L = \frac{L_{bed}}{N_{CSTR}}$) (m)
L_{bed}: packed column length (m)
Nc: number of components (–)
N_{CSTR}: Number of CSTR (continuous stirred tank reactors)
$N_i^{c,j}$: molar flux of component i in the jth CSTR (mol/m^{2}s)
q_{sat}: saturation concentration (mol/m^3 *of crystals*)
q_i: concentration of adsorbed phase (mol/m^3 of *crystals*)
R_c: crystal radius (m)
R_P: pellet radius (m)
T: temperature (K)
v: molar volume of mixture (m^3/mol)
u_f: interstitial velocity (m/s)
ε_i: extra granular porosity (–)
ε_p: intra granular porosity (–)
$\phi_i^{c,j}$: volume fraction of component i adsorbed on solid in the jth CSTR (expressed as a volume fraction of crystal phase) (–)
$\phi_i^{*,j}$: volume fraction of component i in the hypothetical fluid at equilibrium with the adsorbed phase in the jth CSTR (expressed as a volume fraction of the macropores) (–)

$\phi_i^{m,j}$: volume fraction of component i in the macroporosity in the jth CSTR (expressed as a volume fraction of the macropores) (–)

$\phi_i^{f,j}$: volume fraction of component i in the extra-granular fluid phase in the jth CSTR (expressed as a volume fraction of the extra-granular fluid phase) (–)

μ_i: chemical potential (J/mol)

3MP: 3-methylpentane

2MP: 2-methylpentane

22DMB: 2,2-dimethylbutane

TiPB: 1,3,5-triisopropylbenzene

References

Barcia, P.S., Silva, J.A.C., Rodrigues, A.E.: Separation by fixed-bed adsorption of hexane isomers in zeolite BETA pellets. Ind. Eng. Chem. Res. **45**, 4316–4328 (2006)

Boulicaut, L., Brandani, S., Ruthven, D.M.: Liquid phase sorption and diffusion of branched and cyclic hydrocarbons in silicalite. Microporous Mesoporous Mater. **25**, 81–93 (1998)

Calvacante, C.L. Jr., Ruthven, D.M.: Adsorption of branched and cyclic paraffins in silicalite. 2. Kinetics. Ind. Eng. Chem. Res. **34**, 185–191 (1995)

Choudhary, V.R., Akolekar, D.B., Singh, A.P.: Single- and multicomponent sorption/diffusion of hydrocarbons from their iso-octane solution in H-ZSM-5 zeolite. Chem. Eng. Sci. **44**, 1047–1060 (1989)

Jolimaitre, E.: Etude et modélisation de l'adsorption et du transfert de matière dans les zéolithes de structure MFI—application à la séparation des hydrocarbures saturés mono et di-branchés. Thèse de doctorat, Université Claude Bernard, Lyon 1 (1999)

Krishna, R.: Multicomponent surface diffusion of adsorbed species: a description based on the generalized Maxwell-Stephan equations. Chem. Eng. Sci. **45**, 1779–1791 (1990)

Millot, B.: Etude du transport d'hydrocarbures saturés dans des membranes zéolithiques de structure MFI. Thèse de doctorat, Université Claude Bernard, Lyon 1 (1998)

Ruthven, M.: Principles of Adsorption and Adsorption Processes. Wiley, New York (1984)

Schuring, D., Koriabkina, A.O., de Jong, A.M., Smit, B., van Santen, R.A.: Adsorption and diffusion of n-hexane/2-methylpentane mixtures in zeolite silicalite: experiments and modeling. J. Phys. Chem. B **105**, 7690–7698 (2001)

Tayakout, M., Jolimaitre, E., Dubreuil, A.-C., Méthivier, A.: Characterization of multicomponent counter-diffusion in silicalite: application to C6 isomers in liquid phase. In: Proceedings of the AIChE Annual Meeting, pp. 12–17. San Francisco, CA (2007)

Uguina, M.A., Sotelo, J.L., Rodriguez, A., Gomez-Civicos, J.I., Lazaro, J.J.: Liquid adsorption of linear and branched paraffins onto microporous adsorbents—influence of adsorbent structure and Si/Al molar ratio. Sep. Purif. Technol. **51**, 72–79 (2006)

Villadsen, J., Michelsen, M.L.: Solution of Differential Equation Models by Polynomial Approximation. Prentice-Hall, Englewood Cliffs (1978)

Yu, M., Falconer, J.L., Noble, R.D.: Adsorption of liquid mixtures on silicalite-1 zeolite: a density-bottle method. Langmuir **21**, 7390–7397 (2005)